energies

MDPI

Article

Solar Chimney Operation Variant

Marta Gortych [1,*], Zygmunt Lipnicki [1], Tomasz Małolepszy [2] and Piotr Grabas [1]

[1] Institute of Environmental Engineering, University of Zielona Góra, 65-417 Zielona Góra, Poland; z.lipnicki@iis.uz.zgora.pl (Z.L.); p.grabas@adm.uz.zgora.pl (P.G.)
[2] Institute of Mathematics, University of Zielona Góra, 65-417 Zielona Góra, Poland; t.malolepszy@im.uz.zgora.pl
* Correspondence: m.gortych@iis.uz.zgora.pl

Abstract: This paper presents a solar chimney that acts as a heat accumulator. It is based on its alternating charging (melting of the phase change material—PCM) and discharging (solidification), which helps to save energy and ensures stable operation of the solar chimney. In this paper, special attention has been paid to the heat dissipation process (solidification of the PCM). The theoretical model of solidification has been solved in an original way. This paper presents a new simple theoretical model for the solidification of the PCM on a flat plate and presents the results of numerical tests. The theoretical model presents a method for determining the heat transfer coefficient at the solidification front of the PCM. In addition, the heat transfer coefficient from the flowing air to the outer surface of the solidifying front plate was determined experimentally in an original way. The heat transfer coefficient values resulting from the experiments may be employed in order to calculate the heat transfer coefficient for air flowing through the slot of the collector in the solar chimney. The calculated value of the heat transfer coefficient was 18.55 W/m²K.

Keywords: phase change material (PCM); solar chimney; solidification of PCM; heat transfer coefficient; solar heating

check for updates

Citation: Gortych, M.; Lipnicki, Z.; Małolepszy, T.; Grabas, P. Solar Chimney Operation Variant. *Energies* **2024**, *17*, 5004. https://doi.org/10.3390/en17195004

Academic Editor: Antonio Rosato

Received: 23 August 2024
Revised: 23 September 2024
Accepted: 6 October 2024
Published: 8 October 2024

Copyright: © 2024 by the authors. Licensee MDPI, Basel, Switzerland. This article is an open access article distributed under the terms and conditions of the Creative Commons Attribution (CC BY) license (https://creativecommons.org/licenses/by/4.0/).

1. Introduction

The airflow in a solar chimney, which consists of a flat collector with an air gap and a tall central cylinder, is a significant research subject among scientists in the field of heat transfer. A solar chimney can have multiple uses, which include inducing ventilation in buildings, powering an air turbine inside the chimney for electricity generation, and facilitating drying processes. Numerous articles have been published on solar chimneys, mainly discussing experimental research on particular designs and their theoretical analysis. Heat flow theory is typically applied to describe and study actual systems. Some articles also feature analytical models of the movement of air and heat transfer in the solar collector-chimney system.

A solar chimney is a device that functions as a solar energy power plant. Initially, it transforms solar energy to thermal energy through its solar collector. Afterward, it converts this energy into kinetic energy to propel the flowing air up the chimney. Finally, it harnesses the power generated by the wind turbine and generator to produce electricity.

The use of solar energy in solar chimneys helps to reduce greenhouse gas emissions.

The operation of a solar chimney relies solely on solar power. If the sun is not powerful enough, the solar chimney may not work effectively enough to make electricity. Adding a phase change material (PCM) as part of the structure can solve this issue by storing extra heat during periods with more sun and releasing it during periods with less sun, making continuous operation possible. Therefore, suggesting various ways of operating a solar chimney is necessary and appropriate.

One of the earliest works on solar collector and chimney systems is Isidoro Cabanyes' 1903 proposal [1]. His work looked at engine design and proposed the introduction of a solar

air heater attached to a house with a chimney. The inside of the chimney was fitted with an impeller to generate electricity. In 1970, the first combined solar collector and chimney system was designed by Schlaich in Manzanares, Spain [2]. The installation cost is considerable due to the necessity of incorporating a chimney and collector. Furthermore, the power conversion efficiency is notably low. In order to overcome these difficulties, researchers have put forth a number of innovative proposals with the aim of enhancing performance. One potential solution is the selection of an appropriate geometry.

Solar chimney systems have a significant impact on energy supply in nations with abundant solar radiation. Many experts have researched this technology in recent years, specifically exploring solar thermal technology. This type of technology has potential uses globally [1–24].

The European Parliament's climate and energy policy, which aims to reduce greenhouse gas emissions by 2030, has set a target of at least 27% of energy consumed in the EU coming from renewable energy by 2030. In order to reach this target, it is necessary to look for new technical solutions that enable the use of renewable energy sources [25,26]. A good example of this is energy from the sun, which can be used for drying, for example, with a solar chimney.

The article [11] examines the potential of solar chimney systems in combination with other renewable or conventional energy systems. It presents an overview of compact solar chimneys, solar panels, solar ponds, and geothermal energy, as well as an analysis of solar chimney systems, integrated with power plants.

In work [12], a three-dimensional hybrid solar chimney with an integrated external heat source was developed. Solar energy is used for continuous power generation using flue gas channels as a power source in the collector. Extensive numerical studies are also presented. The aim of this article is to theoretically analyze the solidification model of the PCM material on the slab, to analyze the operating conditions of the solar chimney, and to calculate the air heat transfer coefficient.

The origins of solar energy can be traced back 3000 years. Especially deserving of attention are structures from the Middle East. For instance, solar ventilation systems were constructed as early as three thousand years ago in Iran. The main energy driving the movement within these systems is wind power. If wind power is inadequate, solar energy is utilized to heat the walls. This results in a decrease in the density of indoor air, leading to free convection.

Additionally, the use of phase transformation in these constructions is noteworthy. In the building, there were watercourses or reservoirs on the lower floors. Water from the surface of these evaporated, lowering the inside temperature.

Isidoro Cabanyes [4] made an early effort to use solar collector and chimney systems in 1903. He proposed a solar air heater attached to a house with a chimney as part of a motor design. An impeller was installed inside the chimney to produce electricity [4]. Schlaich conceptualized the solar collector and chimney arrangement in 1970, at Manzanares, Spain. The chimney had a height of 195 m and a diameter of 10 m, and the collector's radius was 122 m. The prototype was a miniature experimental version. In its final form, it produced approximately 50 kW [2]. In 1995, Schlaich suggested an innovative method to create a solar collector stack, where the gadget obtains power from direct and diffused radiation, as well as from the soil's heat accumulation. The collector and stack were fashioned utilizing basic elements and techniques [15]. In the paper [27], a numerical study was presented, which examined the impact of varying chimney shapes, including round, convergent, divergent, abrupt contraction, and abrupt expansion, on the performance of a solar chimney power plant (SCPP). Moreover, the parametric effect of varying chimney divergence angles and ground absorber inclination angles on the performance of a solar chimney power plant (SCPP) was also examined. The optimal divergence angle was identified. The findings of their study were benchmarked against those of the classical Manzanares power plant, which demonstrated an increase in energy production of up to 80% (92 kW) relative to the Manzanares plant.

The objective of the paper [28] is to review SCPPs in order to gain insight into the underlying physics of the flow and to identify the key parameters and their values that are most pertinent to the optimal design of an SCPP. Additionally, hybrid models with further modifications that are suitable for commercial production of large-scale SCPPs are included.

In sunnier countries, solar chimneys have a vital role in supplying energy. Therefore, in recent decades, loads of researchers have delved into solar chimney systems, exploring them as a way of producing solar thermal energy that could be used globally. Bernardes and colleagues (2012) conducted a thorough analysis of different models to determine the performance of a solar collector stack. The aim was to estimate the output of solar chimneys and to examine how varying environmental conditions and geometric dimensions affect the output of solar chimneys. The mathematical model was verified through experiments and used to predict how commercial solar chimneys will perform. Stack height, turbine pressure drop and diameter features were discovered to be very important [4].

The paper [29] reviews the thermodynamic principles underlying the energy balance equations of the plant and those needed for the various components, as these principles are useful for design calculations. Furthermore, exergy analysis and cost estimation are also discussed. A review of the global status of power plants over the past two decades reveals that the system capacity potential ranges from 0.053 to 27 MW. Any mathematical analysis and research gaps were summarized, as they are useful for informing future research. Additionally, the factors affecting system performance, including area transfer coefficients, pressure profile, and turbine pressure drop, were provided. The main challenges encountered at the plant were identified as lower thermal efficiency, site requirements for a commercial plant, and the construction of a tall chimney. In conclusion, recommendations and prospects for the future of the plant were presented.

An intriguing paper is that of Saleh et al. [30], which presents a review of current literature examining the performance of the primary components of solar chimney power plants and the most effective approaches to enhance the system's performance through diverse methodologies. These include the incorporation of the system with heat storage materials and phase change materials (PCMs), as well as its integration with other technologies. Additionally, the paper discusses the integration of solar chimney power plants with external heat sources and engineering solutions for tower chimney design, with the objective of optimizing the performance of solar chimney power plants.

In the article by Lipnicki et al. [7], the authors suggest a new way to solve the problem of air flow through solar collectors and chimneys. They use the classical system of conservation equations (momentum, mass, and energy) and similarity theory. This method allows the making of a solar chimney. The theoretical analysis was compared to experiments conducted on current solar chimney and solar collector systems. The experimental and theoretical studies were found to be sufficiently consistent. The flow of heat in a solar chimney was outlined at length, using dimensionless numbers, including Reynolds, Grashof, Galilean, Biot, and Prantdl numbers.

The paper deals with the solidification of a PCM material in the form of a flat disc with radius R and height H. The paper presents heat accumulation by melting the PCM material and heat release by the solidification of the PCM material, along with a new theoretical model for the solidification of PCM on a flat plate, presenting the results of numerical tests. The theoretical model presents a method for determining the heat transfer coefficient at the solidification front of the PCM. In addition, the heat transfer coefficient from the flowing air to the outer surface of the solidifying front plate was determined experimentally in an original way. Chapter two presents a theoretical model for the solidification of a PCM material in the form of a flat plate, introduces a mini solar chimney, and shows its construction and the variation possibilities of the operation of this chimney. Chapter three presents the results of numerical calculations of the solidifying slab of PCM material, and the heat transfer coefficient is determined and presented.

This work solves a new problem about solar chimney operation. It looks at heat accumulation in PCM using phase transformation. This problem has not been considered in the scientific literature.

2. Materials and Methods

2.1. Theoretical Model of Solidification of PCM Plate

Figure 1 shows the one-dimensional solidification model in the z direction, directed opposite to the acceleration vector of gravity g, for a flat liquid layer of PCM material of thickness H, thermally insulated from the top and cooled from the bottom by air flowing at a temperature T_a and at a velocity u. A very small gap, called the contact layer, is formed between the lower plate made at the temperature T_W of a very good conductor (copper) and the solidified PCM material, which creates additional resistance to heat flow q. The resulting gap in contact with the solidified layer has a temperature of T_C. A solidified layer of thickness δ develops on the lower plate. The non-solidified liquid layer of thickness $H - \delta$ decreases with time t and is assumed to be immovable (no free convection).

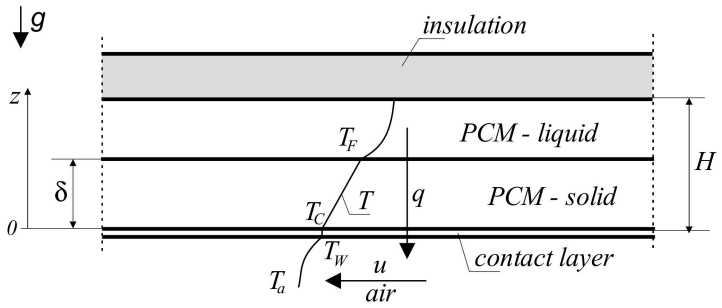


Figure 1. Solidification model of the PCM plate.

The lack of free convection in the liquid layer justifies the expected temperature distribution. The lower liquid layers have a lower temperature and therefore a higher density, which does not favor the formation of free convection.

Such a simplified description of the solidification phenomenon justifies its relatively long duration [5,31].

$$h_F\left(\overline{T}_L - T_F\right) + \rho_S L\frac{d\delta}{dt} = k_S\frac{T_F - T_C}{\delta} = h_{CON}(T_C - T_W) = h(T_W - T_a) \quad (1)$$

The first term of the above equation represents the sum of the heat fluxes: transferred from the liquid with the transfer coefficient h_F, where $\overline{T}_L$ is the average temperature of the liquid, and T_F represents the solidification temperature and the heat of phase change, where ρ_S is the density of the solidified layer, and L denotes the heat of solidification. The second term of the equation represents the heat flux flowing through the solidified layer. The third term represents the heat flux flowing through the contact layer, with the transfer coefficient h_{CON}. The fourth term represents the heat flux transferred by the cooling air flow with the transfer coefficient h.

The heat stream absorbed from the superheat liquid PCM is equal to the capacitive heat change in the plate of the liquid in the duration phenomena

$$h_F(\delta)\left(\overline{T}_L - T_F\right) = -\frac{d}{dt}\left[(H - \delta)\rho_L c_L\left(\overline{T}_L - T_F\right)\right] \quad (2)$$

The above equation is derived from the heat balance of a PCM board.

The subject of this work is the solidification of a liquid placed in a plate space. The space is shown in Figure 1. In the space, the solidification flat front with thickness $\delta(t)$ moves from the flat cooling surface to the outer surface of the thickness H. The inner surface with $z = 0$ is cooled by the flowing coolant air. The heat stream of solidification $\dot{q}$ flows into the air.

The quasi-stationary equation describing in flat space the temperature fields both in the liquid space $\delta(t) \leq z < H$ and in the solidified layer space $0 \leq z \leq \delta(t)$ describes the same quasi-stationary differential equation:

$$\frac{d^2T}{dz^2} = 0. \tag{3}$$

The boundary conditions are equal:

- For the solidified layer in the space $0 \leq z \leq \delta(t)$:

$$T = T_F \; for \; z = \delta, \text{ and } T = T_C \; for \; z = 0. \tag{4}$$

- For the stand still liquid in the space $\delta(t) \leq z < H$

$$T = T_F \text{ and } \overline{T}_L(t) = \frac{\int_\delta^H T(z)dz}{H-\delta} \; for \; z = \delta, \tag{5}$$

where the average temperature of the liquid is given by

$$\overline{T}_L - T_F = \frac{\int_\delta^H [T(z) - T_F]dz}{H-\delta}. \tag{6}$$

In the solidified layer $0 \leq z \leq \delta(t)$, the temperature distribution and the stream heat are equal:

$$T = T_C + (T_F - T_C)\frac{z}{\delta} \tag{7}$$

$$\dot{q}_S = -k_S \left.\frac{\partial T}{\partial \hat{z}}\right|_{\hat{z}=\delta} = -k_S \frac{T_F - T_C}{\delta}. \tag{8}$$

In the liquid space $\delta(t) < z < H$, the temperature distribution and the stream heat on the solidification front are equal:

$$T = \frac{2\left(\overline{T}_L - T_F\right)}{H-\delta} z + T_F \frac{H+\delta}{H-\delta} - \frac{2\delta}{H-\delta}\overline{T}_L, \tag{9}$$

$$T(\delta) = \frac{T_F(H-\delta)}{H-\delta} = T_F$$

$$\dot{q} = -k_L \left.\frac{\partial T}{\partial z}\right|_{z=\delta} = k_L \frac{2\left(\overline{T}_L - T_F\right)}{H-\delta}. \tag{10}$$

The stream of heat absorbed from the liquid to the solidification front is equal:

$$\dot{q} = h_F(\delta)\left(\overline{T}_L - T_F\right). \tag{11}$$

Comparing heat streams, the heat transfer coefficient on a cylindrical surface with a thickness δ on the liquid side is equal:

$$h_F(\delta) = \frac{2k_L}{H-\delta}. \tag{12}$$

After the appropriate transformation of equations (1), one equation of heat flux balance was obtained:

$$h_F\left(\overline{T}_L - T_F\right) + \rho_S L \frac{d\delta}{dt} = k_S \frac{h_{CON} h}{h_{CON} k_S + h k_S + h_{CON} h \delta}(T_F - T_a). \tag{13}$$

The system of differential Equations (1)–(3) can be replaced by the following dimensionless system:

$$2\frac{\widetilde{k}B}{1-\widetilde{\delta}}\overline{\theta}_L + \frac{d\widetilde{\delta}}{d\tau} = \frac{Bi_a Bi_{CON}}{Bi_a + Bi_{CON} + Bi_a Bi_{CON}\widetilde{\delta}}, \tag{14}$$

$$2\frac{\widetilde{a}}{1-\widetilde{\delta}}\overline{\theta}_L = -Ste\frac{d}{d\tau}\left[\left(1-\widetilde{\delta}\right)\overline{\theta}_L\right], \tag{15}$$

by introducing dimensionless quantities into the above equation system: thickness of the solid layer $\widetilde{\delta} = \delta/H$, time $\tau = Fo\ Ste$, the average overheat temperature of the liquid $\overline{\theta}_L = \left(\overline{T}_L - T_F\right)/(T_{L0} - T_F)$, where T_{L0} is the initial temperature of liquid PCM material, $Fo = a_S t/H^2$ is the Fourier number, $Ste = c_S(T_F - T_a)/L$ is the Stefan number, $a_S = k_S/(\rho_S c_S)$ is the thermal diffusion coefficient of the solidified layer, $a_L = k_L/(\rho_L c_L)$ is the liquid thermal diffusion coefficient, $Bi_{CON} = h_{CON}H/k_S$ is the Biot number in the contact layer, $Bi_a = hH/k_s$ is the Biot number on the surface of the plate, $B = (T_{L0} - T_F)/(T_F - T_a)$ is the liquid overheat parameter, $\widetilde{a} = a_L/a_S$ is the ratio of liquid and solid heat diffusion coefficients, $\widetilde{k} = k_L/k_S$ is the ratio of the heat conduction coefficients of the liquid and solid.

The system of differential equations above satisfies the initial conditions:

$$\widetilde{\delta} = 0, \qquad \overline{\theta}_L = 1\ for\ \tau = 0. \tag{16}$$

These conditions can be found numerically.

For small overheating parameters $B \to 0$ (see the figure in Section 3.1), which occur in reality, there is no significant difference in the change of the solidified layer thickness; therefore, the simple equations below can be used in the solidified layer thickness and in the solidification velocity calculations.

Hence, Equation (14) leads to simple equations of the solidified layer thickness [5]:

$$\widetilde{\delta} = -\left(\frac{1}{Bi_a} + \frac{1}{Bi_{CON}}\right) + \sqrt{\left(\frac{1}{Bi_a} + \frac{1}{Bi_{CON}}\right)^2 + 2\tau} \tag{17}$$

and the solidification velocity is given as follows:

$$\frac{d\widetilde{\delta}}{d\tau} = \frac{1}{\sqrt{\left(\frac{1}{Bi_a} + \frac{1}{Bi_{CON}}\right)^2 + 2\tau}}. \tag{18}$$

Equations (17) and (18), after performing the transformations, allow us to determine the thickness of the solidified layer (δ) and the heating power $\left(\dot{Q}\right)$:

$$\delta = H\ \widetilde{\delta}\ \text{and}\ \dot{Q} = \frac{\rho_S L a_S}{H} Ste\ F\ \frac{d\widetilde{\delta}}{d\tau}. \tag{19}$$

2.2. The Mini Solar Chimney

The mini solar chimney that inspired this work was created as part of the project titled "Cooperation of scientific partners in education and knowledge exchange in the field of energy storage technology and energy efficiency in the SNB region", co-funded by the INTERREG VA Brandenburg—Poland 2014—2020 program. The mini solar chimney is located in the premises of the Centre for Education in Energy Storage Technology in the field of thermal energy storage and energy efficiency, located in Nowy Kisielin, in the Science and Technology Park of the University of Zielona Góra. Figure 2 shows a photo of the mini solar chimney.



Figure 2. Chimney test bench.

Figure 3 shows a schematic diagram of a mini solar chimney, which consists of two main parts: a solar collector and a vertical thermally insulated pipe placed in the center of the panel.

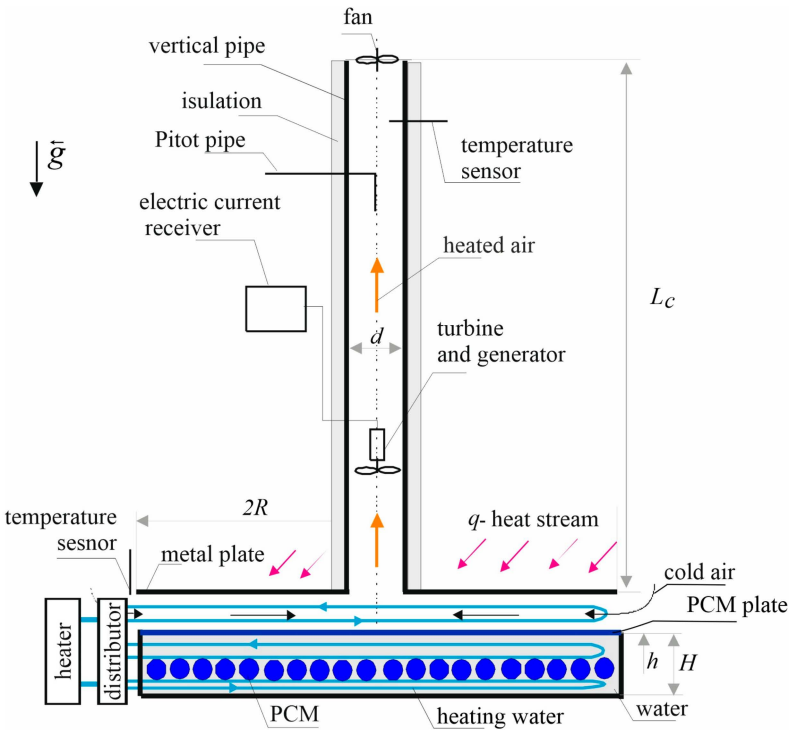


Figure 3. Construction diagram for a mini solar chimney.

Due to its size, the mini-chimney's performance is not significant. However, obtaining practical research results using thermodynamic similarity principles may be useful for real, large-scale solar chimneys. The theoretical and practical outcomes of the small chimney can aid in the development of real chimneys, and it is clear that the cost of experimental studies on a small chimney is not high compared to the cost of working on large solar chimneys. Solar chimneys are not profitable in Poland, but they can be used as an example for other countries with more sunlight.

The solar panel consists of two flat disks horizontally positioned at a height of H and parallel to each other, with a space in between, called an air gap h. The top plate is made of metal and has a specific diameter of 2R = 2000 mm, an air gap width of h = 80 mm, and

a distance between two parallel flat disks of $H = 470$ mm. In the middle of the concrete surface sat a vertically positioned, heat-resistant tube with an inner diameter of d = 100 mm and a height of Lc = 2500 mm (Figure 3). Depending on the research requirements, the pipe could be substituted with a longer one. Moreover, the illustration displays further measurement and testing components: a water heater with manifold and metal coils, spheres containing PCM material, and a flat PCM material plate. The standpipe may have a turbine power generator, for example, attached within, and an axial fan installed at the very top to reinforce the airflow. Sensors are appropriately placed within the pipe to gauge the airflow and temperature.

Due to the heating of the air from the sun, radiant heat, a water heater, or the solidification of PCM material within the chimney, an air flow known as the "chimney effect" emerges in the solar collector—chimney (standpipe) system. An instrument called a wing anemometer was utilized to measure the air velocity within the chimney, while a thermometer was employed to measure the temperature. For example, the air velocity measurements using the wing anemometer were compared to those made with the Pitot tube in the chimney. In addition, we measured the pressure drop at the junction between the collector and standpipe with a Recknagel differential pressure gauge. The pressure drop at the junction between the solar collector and the standpipe represents the local loss of airflow, as defined in the context of fluid mechanics. These results were the subject of a previous paper by the authors [7]. We used a radiation sensor at a nearby meteorological station to measure solar radiation.

All the measurements of the solar chimney's functioning were saved using the Building Management System (BMS), as shown in Figure 4. The BMS tracks the temperature at two points of the chimney, the air flow in the chimney, and the temperature at the top and bottom of the collector container, as well as the power that is consumed and the active power.

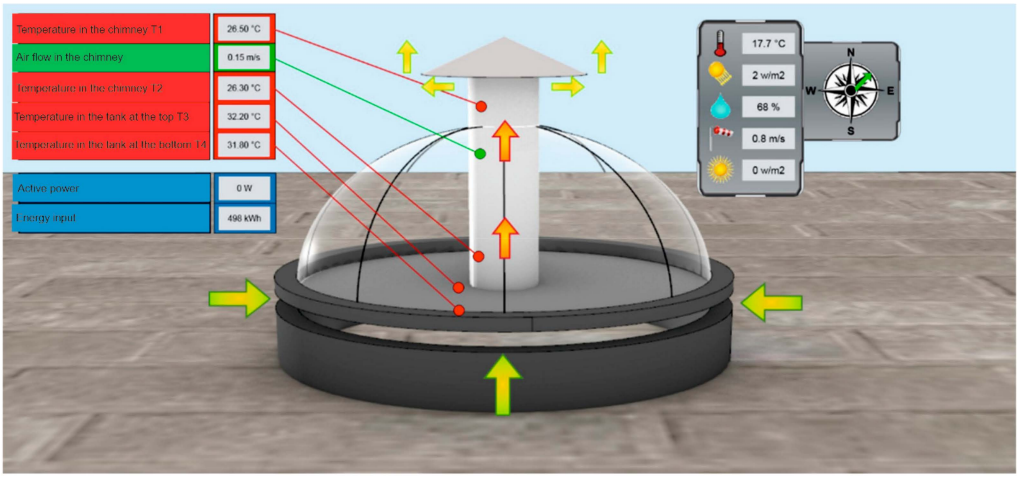


Figure 4. BMS visualization of solar chimney operation.

In addition, external parameters can be read from a nearby meteorological station, including the temperature, the total and diffuse solar radiation, humidity, as well as wind speed and direction.

The mini solar chimney has been designed and manufactured in such a way that it can be used to test different configurations and heat flows. The mini solar chimney allows the multi-dimensional operation of such a system to be represented, i.e., the use of the solar heat flow, the use of the heat exchanger, and the use of the heat flow of the PCM material. This is possible thanks to a system of three exchangers (coils) installed in the mini solar chimney. The following are the heat exchangers:

- The first one is placed on the bottom plate of the solar collector, within the space of the flowing air. In this case, the air in the gap of the solar collector is heated by the heat of the solar radiation.
- The second one is placed in the tank space under the solar collector, where the PCM material is placed, which works in two cycles:
- Melting of the PCM material by the warm air flowing in the collector gap (charging of the storage tank);
- Solidification of the PCM material by the cold air flowing in the collector gap (discharging the heat storage tank).
- The third is at the bottom of the tank, under the solar collector. In this case, the air in the collector gap is heated by the heat from the heat exchanger.
- The solar chimney co-operates with a round flat plate of phase change material (PCM), which solidifies when air flows through the collector gap. The solidification process of the liquid PCM material is shown in Figure 5.
- The air flowing in the collector gap has a velocity u and an average temperature $\overline{T}_p$ lower than the solidification temperature T_F of the PCM material. As a result of the process of absorbing heat $\dot{q}$ from the liquid, it is in the form of a cylindrical plate, with a radius R and a thickness H, where the solidification process of the PCM material takes place.

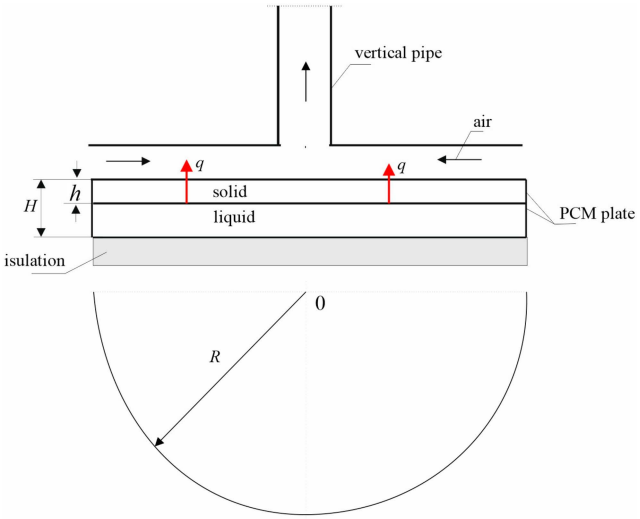


Figure 5. Integration of a mini solar chimney with a solidifying plate.

3. Results and Discussion

This section is divided into three subsections: 3.1. Solidification of PCM Plate, 3.2. Determination of the Heat Transfer Coefficient, 3.3. Examples of Mini-Chimney Operation Processes.

3.1. Solidification of PCM Plate

Numerical solutions of the integral in Equations (14) and (15) for different parameters are presented in Figure 6a,b.

Figure 6a shows the thickness of the solid layer over time, Figure 6b depicts the average overheat temperature of the liquid over time. The presented figures indicate that the thickness of the slid layer increased, and the average overheat temperature of the liquid decreased over time. The influence of the overheating parameter B on the temperature distribution is insignificant.

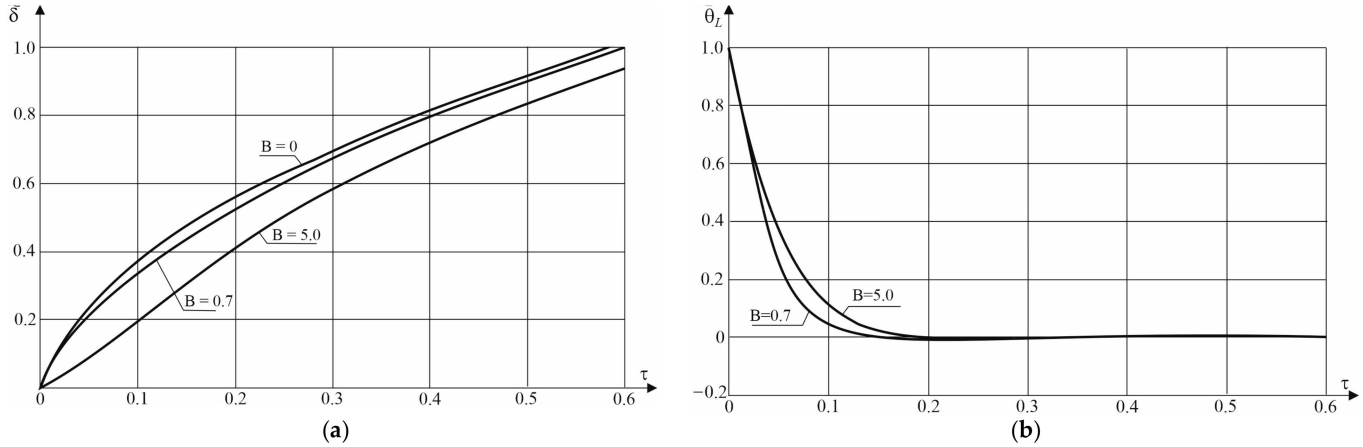


Figure 6. Numerical results for the system defined by Equations (13) and (14) with parameters $\left(Bi_{CON} = 160, Bi_a = 12.5, Ste = 0.112, \widetilde{a} = 1.13, \widetilde{k} = 1\right)$ for various values of B, (**a**) the thickness of the solid layer over time, (**b**) the dependence of the average temperature over time.

Figure 7 shows the thickness of the solid layer over time for different Biot numbers (Bi_a) on the air side for $B = 0$.

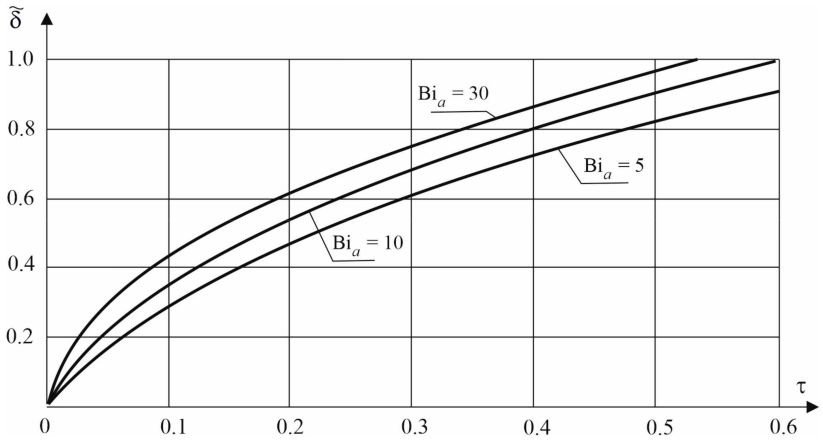


Figure 7. The thickness of the solid layer over time for $B = 0$.

The solidified layer became thicker over time, with more the Biot numbers on the surface of the plate Bi_a.

3.2. Determination of the Heat Transfer Coefficient

A very important thermodynamic parameter for the air flowing in the solar collector gap is the heat transfer coefficient (h). In order to determine it, original experimental research was carried out on a test bench constructed by the co-author of the paper and shown in Figure 8a. The diagram of the test bench is shown in Figure 8b. The test stand consists of a tank with a radius of $R = 63.5$ mm and a height of $H = 104$ mm, and it is made of acid-resistant steel, with a wall thickness of 1.5 mm and a mass of $m_s = 0.695$ kg. The mass of the water in the tank is $m = 1$ kg, and the temperature is T_w. The results of the measurements are recorded for different initial temperatures T_{wp}. The water tank is installed in a 247 mm diameter duct (Figure 8), in which the air flows at a temperature of T_p. There is a heater under the duct. The heater heats the air at different flow rates (u).

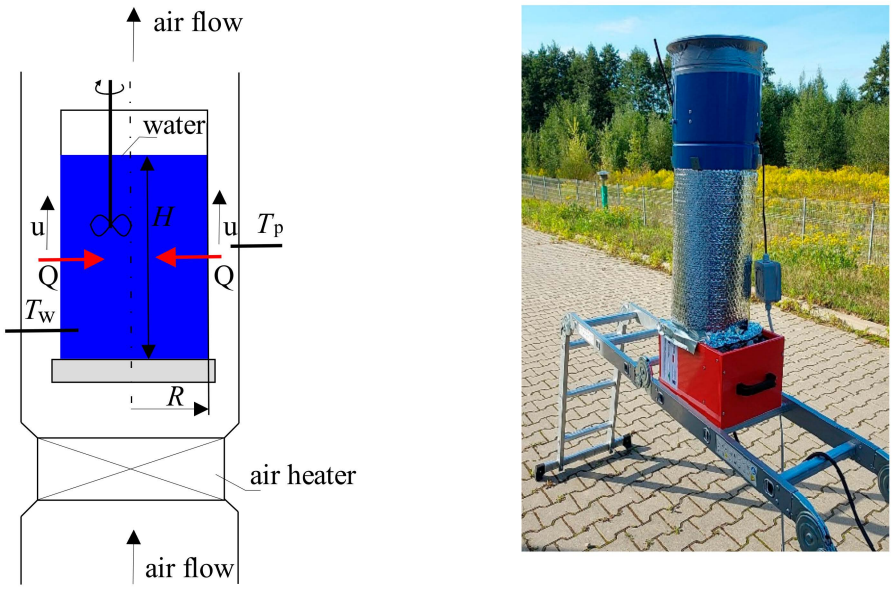


Figure 8. Scheme (**a**) and the photo (**b**) of the research unit.

The temporary heat balance of the tank is described by the formula

$$dQ = (mc_w + m_s c_s)dT_w = h(T_p - T_w)Fdt \tag{20}$$

where h—the heat transfer coefficient, c_w—the specific heat of the water, c_s—the specific heat of the solidified layer, F—the side surface of the tank ($F = 2\pi RH$).

By separating the variables, an ordinary differential equation was obtained:

$$-(mc_w + m_s c_s)\frac{d(T_p - T_w)}{T_p - T_w} = hFdt, \tag{21}$$

whose solution is given when the initial condition is satisfied: $t = 0$, and $T_w = T_{wp}$ is the equation

$$T_w = T_p - (T_p - T_{wp}) \cdot exp(-At), \tag{22}$$

where $A = \frac{hF}{mc_w + m_s c_s}$.

The average simplified heat balance for a container of water over time t is equal to

$$m_w c_w (T_{wk} - T_{wp}) + m_s c_s (T_{wk} - T_{wp}) = h(T_p - \overline{T}_w)Ft, \tag{23}$$

where $\overline{T}_w = \frac{T_{wp} + T_{wk}}{2}$ is the average water temperature, T_{wp} is the initial water temperature, T_{wk} is the final water temperature, $F = 2\pi RH$ is the side surface of the tank, and t is the time.

The heat transfer coefficient, which also takes into account the heat absorbed by the tank wall, is

$$h = \frac{m_w c_w (T_{wk} - T_{wp}) + m_s c_s (T_{wk} - T_{wp})}{(T_p - \overline{T}_w)Ft} = 18.55\frac{W}{m^2 K}. \tag{24}$$

It is assumed that the temperature of the water is equal to the temperature of the vessel wall.

By substituting the values of the h parameters from Equation (24) into parameter A, the time variation of the water temperature is described by the equation:

$$T_w = T_p - (T_p - T_{wp})e^{-At} = 62.9 - (62.9 - 31.94)e^{-0.000184\ t} \tag{25}$$

Equation (25) shows the variation of the water temperature with time as a function of the ambient air temperature ($T_{p)}$ and the initial temperature of the water (T_{wp}). The constant A represents the ratio of the heat transfer coefficient and the external surface area of the tank to the sum of the products of the mass of water and its specific heat and the mass of the solidified layer and its specific heat.

As can be seen in Figure 9, the temperature profile as a function of time is linear (straight line). Therefore, the simplified method presented in this paper can be used to calculate the heat transfer coefficient on the side surface of the tank.

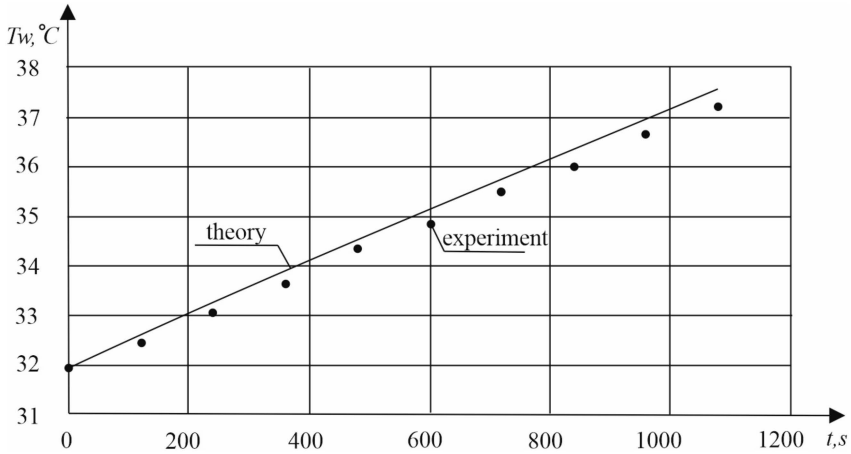


Figure 9. Comparison of the results of experimental and theoretical studies of temperature versus time measurements.

The values of the heat transfer coefficient obtained from the experiments carried out can be used to calculate the heat transfer coefficient for the air flowing in the collector slot in the solar chimney. An additional assumption must then be made that the curvature of the cylindrical surface $(1/R)$ is small. Heat transfer coefficient values h (Figure 10). They increase as the velocity of the flowing air increases. The test results obtained can be used to determine the conditions of heat transfer in the flat gap of a solar collector.

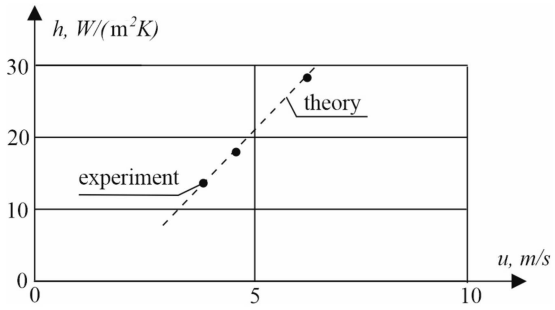


Figure 10. Dependence of the coefficient of heat transfer on the velocity of the air.

The results of the experimental and theoretical studies are presented in a graph (Figure 10).

3.3. Examples of Mini-Chimney Operation Processes

In a research study [6], a solar chimney was examined both theoretically and experimentally, and the optimum operating conditions were established based on the authors' original research (refer to Figures 11 and 12).

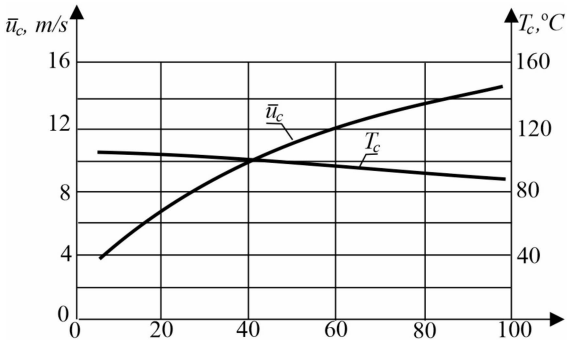


Figure 11. Dependence of velocity $(\bar{u}_C)$ and temperature (T_C) of air in chimney on chimney stack height (H_C) for a heat flow of $\dot{q} = 800$ W/m^2 [6].

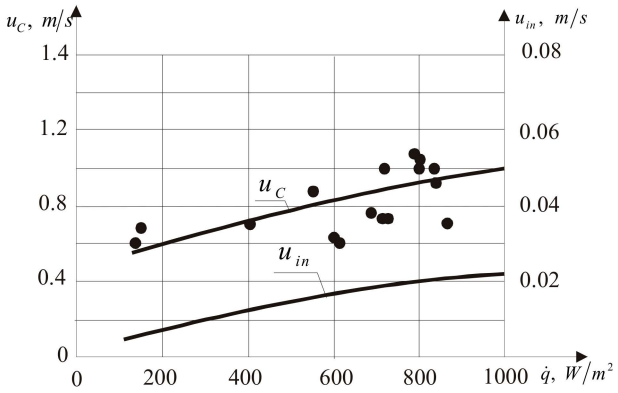


Figure 12. Comparison of air velocity in the theoretical model chimney with experimental tests for a mini-chimney [6].

The data obtained from the operation of the mini solar collector, comprising measurements of air flow speed in the chimney, wind speed, sunlight, and air temperature, are presented in tabular form in Table 1.

Table 1. Summary of operating parameters of the mini solar chimney.

Date/Time	Air Flow Velocity in the Chimney [m/s]	External Wind Speed [m/s]	Insolation [W/m^2]	Air Temperature [°C]	Air Flow Velocity in the Chimney [m/s]
8 February 2020	0.7	25	279.2	4.1	0.7
11 February 2020	1.1	7.2	164.9	5.8	1.1
2 September 2022	2.1	1.0	846.6	21.2	2.1
3 September 2022	0.6	0	2	14.1	0.6

The test results presented in Table 1 demonstrate that the air velocity within the chimney is contingent upon solar radiation, air temperature, and external wind speed. In general, the air velocity in the chimney increases with increasing solar radiation. The presence of dust in the chimney is a significant parameter affecting the speed of the air flow. The chimney contains dust on the top plate of the solar collector; therefore, it is essential to ensure that the collector plate is kept clean. The mini solar chimney, as the name suggests, achieves a low output; however, the results obtained from its operation can be useful for chimneys with large external dimensions.

3.3.1. Heating the Air in the Collector Gap with the Heat of the Solidification Stream

The influence of the heat transfer coefficient (h) on the thickness of the solidified layer is shown in Figure 13. The curves shown in the figure are the graphical form of Equation (16).

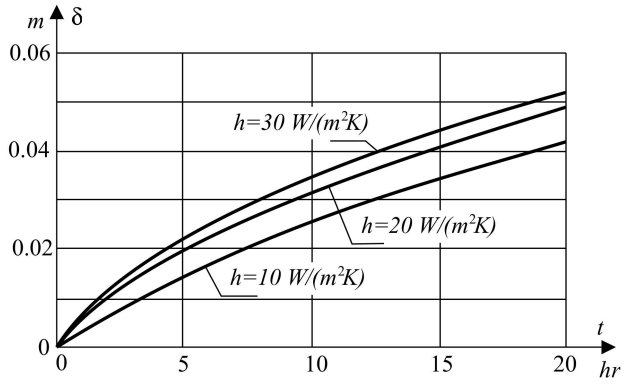


Figure 13. The influence of the heat transfer coefficient on the thickness of the solidified layer for different values at the plate, with $Bi_{CON} = 160$.

As the value of the heat transfer coefficient increases, the thickness of the solidified layer increases more rapidly.

3.3.2. The Heat Flow from the Flat Lower Circular Plate in the Collector Gap

The PCM material was used to calculate the heat flow from the flat-bottomed circular plate in the collector slot.

The PCM used was Rubitherm®RT64HC, with the following thermophysical parameters: the solidification heat, $L = 250$ kJ/kg; the thermal conductivity coefficient, $k_s = 0.2$ W/(mK); the density of the solid, $\rho_S = 880$ kg/m^3; the density of the liquid $\rho_L = 780$ kg/m^3; the specific heat capacity $c_p = 2.0$ kJ/(kgK); the heat diffusion coefficient, $a_S = 1.25{\cdot}10^{-7}$ m^2/s; density, $\rho_s = 880$ kg/m^3 [24].

The parameters of the PCM plate were the following: the radius of the plate, $R = 1$ m; the plate temperature, $T_w = 64$ °C; the surface area of the plate, $F = 1$ m^2.

The air parameters in the gap were as follows: the air velocity, $u = 1.5$ m/s; the average air temperature, $\overline{T_a} = 20$ °C; the coefficient of kinematic viscosity, $\nu = 15.06{\cdot}10^{-6}$ m^2/s; the heat conductivity of the air, $k_a = 2.59{\cdot}10^{-2}$ W/(mK); the Prandtl number, $Pr = 0.703$.

The growth rate of the solidified layer $d\delta(t)/dt$ (indirectly representing the heat flux density) and the increase in thickness of the solidified layer $\delta(t)$ over time according to Equation (16) are shown in Figures 14 and 15.

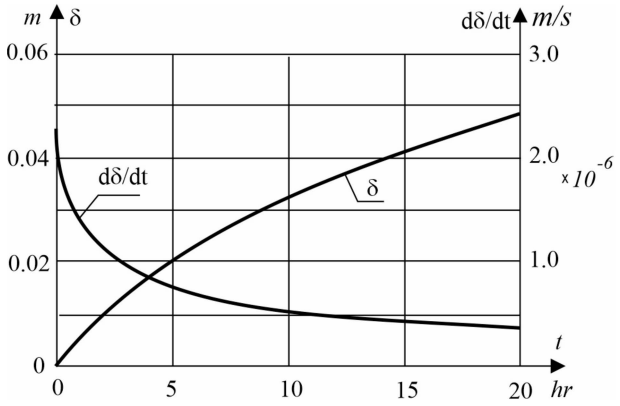


Figure 14. The increase in the thickness of the solidified layer and the rate of solidification as a function of time for $h = 20$ W/(m^{2}K) and $Bi_{CON} = 160$.

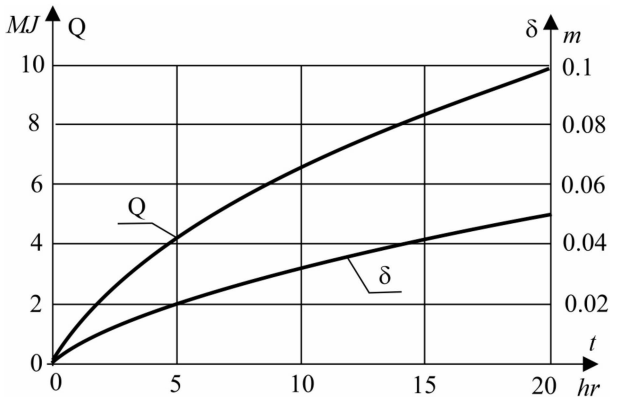


Figure 15. Heat released from a layer that has solidified over time, for $h = 20\ \mathrm{W/(m^2K)}$ and $Bi_{CON} = 160$.

As can be seen in Figure 14, the thickness of the solidified layer increases during the solidification process, while the solidification rate decreases. The highest solidification rate occurs at the beginning of the process.

The heat released as the phase of the PCM material changes over time is shown in Figure 16. This process can be thought of as discharging the heat storage. Figure 16 also shows the increase in thickness of the solidified layer over time.

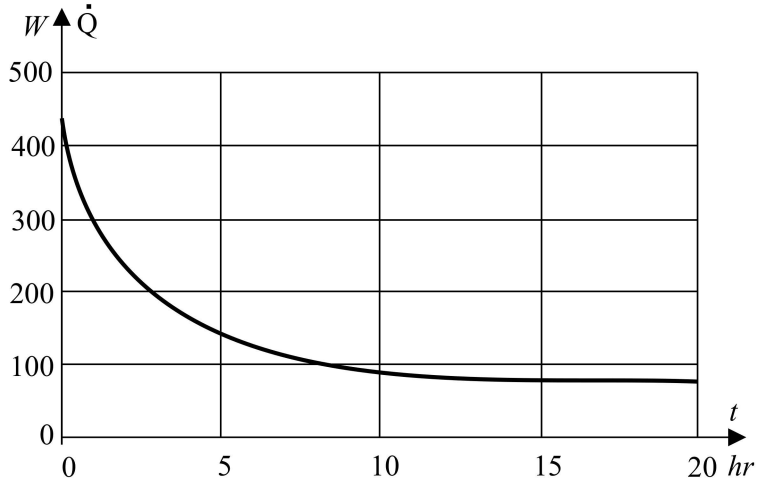


Figure 16. Total heat flow as a function of time for $h = 20\ \mathrm{W/(m^2K)}$ and $Bi_{CON} = 160$.

As depicted in the figure above, both the total amount of heat released and the thickness of the solidified layer increase with time.

The total heat flux released in the solidification process, calculated according to equation 12 for a collector plate with the surface of $F = 1\mathrm{m}^2$, is shown in Figure 16.

As can be seen in Figure 16, the total heat flux (power) decreases during the process. This is due to the increase in thickness of the solidified layer and therefore, the increase in thermal resistance of the solidified layer.

4. Conclusions

The multi-variant operation of the mini solar chimney, as presented in this paper, demonstrates in a straightforward manner that external heat can be converted into air movement in a number of different ways. Solar radiation, or radiation from a radiator, can be employed directly to heat the air flowing in the gap between the solar collectors. This particular configuration of a solar chimney represents a classic example of such a device, and it is comprehensively documented in the technical literature. In reference [6], a comprehensive and insightful theoretical analysis of the solar chimney operation was conducted.

The process presented in this work on solar chimney operation is comprised of two stages. The initial stage entails utilizing solar radiation to impart kinetic energy to the airflow within the solar chimney, while simultaneously facilitating the melting of the PCM material. The melting of the PCM material is associated with the charging of excess energy. In the second stage, in the absence of solar radiation, the energy accumulated in the PCM material is returned to the air flowing in the chimney as a result of the PCM material solidification process. This work provides a detailed analysis of the solidification process. The two stages are repeated cyclically. The proposed method of chimney operation is continuous and stable. During the nocturnal period, when solar radiation is absent, the solar chimney operates continuously, maintaining a constant temperature throughout the heat exchange process.

The solution presented in this work is highly beneficial for environmental protection. Furthermore, the work presents an original method of determining the heat transfer coefficient between the flowing air and the flat plate of the solar collector.

The achievements of this work include experimental studies on the heat transfer coefficient between the air flowing in the gap and the surface of the collector plate. There is a lack of theoretical studies in the scientific literature on the heat transfer coefficient for axially symmetric air flows over flat plates, which should be the focus of further theoretical and experimental research.

It is best to build solar chimneys in countries with a warm climate and plenty of sunlight. In our country, the climatic conditions are rather unfavorable for building large chimney construction investments. However, the theoretical research carried out on a mini-chimney and the results obtained can be transferred to large chimneys, using a similarity scale.

Author Contributions: Conceptualization, M.G., Z.L., T.M. and P.G.; methodology, M.G., Z.L., T.M. and P.G.; validation, M.G. and Z.L.; formal analysis, M.G., T.M. and Z.L.; investigation, M.G., P.G. and Z.L.; resources, M.G., P.G. and Z.L.; data curation, M.G., Z.L., T.M. and P.G.; writing—original draft preparation, M.G. and Z.L.; writing—review and editing, M.G. and Z.L.; visualization, M.G. and Z.L.; supervision, M.G. and Z.L. All authors have read and agreed to the published version of the manuscript.

Funding: This research received no external funding.

Data Availability Statement: The original contributions presented in the study are included in the article, further inquiries can be directed to the corresponding author.

Conflicts of Interest: The authors declare no conflicts of interest. The funders had no role in the design of this study; in the collection, analyses, or interpretation of data; in the writing of the manuscript; or in the decision to publish the results.

Nomenclature

a_S	thermal diffusivity of the solidified layer, $\mathbf{m^2/s}$
a_L	thermal diffusivity of the liquid, $\mathbf{m^2/s}$
c_S	specific heat of the solidified layer, $\mathbf{J/(kgK)}$
c_L	specific heat of the liquid, $\mathbf{J/(kgK)}$
g	gravity of acceleration, $\mathbf{m/s^2}$
h	heat transfer coefficient at the plate, $\mathbf{W/(m^2K)}$
h_F	heat transfer coefficient at the solidification front, $\mathbf{W/(m^2K)}$
h_{CON}	heat transfer coefficient at the contact layer, $\mathrm{W/(m^2K)}$
k_L	heat conductivity of liquid, $\mathrm{W/(mK)}$
k_S	heat conductivity of the solidified layer,$\mathrm{W/(mK)}$
k_C	heat conductivity of cooling liquid,$\mathrm{W/(mK)}$
H	plate PCM material height, m

L	latent heat of liquid, J/kg
k	heat conductivity, W/(mK)
L_C	chimney length, m
$\dot{q}$	heat flux, W/m^2
$\dot{Q}$	heat transfer rate, W
t	time, s
T	temperature, K
u	velocity, m/s
z	coordinate, m
Greek symbols	
δ	thickness of the solid layer, m
ρ	density, kg/m^3
$\overline{\theta}_L$	overheat temperature of the liquid
τ	time

References

1. Asnaghi, A.; Ladjevardi, S.M. Solar chimney power plant performance in Iran. *Renew. Sustain. Energy Rev.* **2012**, *16*, 3383–3390. [CrossRef]
2. Haaf, W.; Friedrich, K.; Mayr, G.; Schlaich, J. *Solar Chimneys—Part I: Principle and Construction of the Pilot Plant in Manzanares*; Taylor & Francis: Abingdon, UK, 1983; pp. 3–20.
3. Bernardes, M.A.d.S.; Voß, A.; Weinrebe, G. Thermal and technical analyses of solar chimneys. *Sol. Energy* **2003**, *75*, 511–524. [CrossRef]
4. Cabanyes, I. Proyecto de Motor Solar. *Energ. Eléctrica—Rev. Gen. Electr. Sus Apl.* **1903**, *8*, 61–65.
5. Lipnicki, Z. *Dynamics of Liquid Solidification, Thermal Resistance of Contact Layer*; Mathematical Engineeringm; Springer International Publishing: Cham, Switzerland, 2017.
6. Lipnicki, Z.; Gortych, M.; Staszczuk, A.; Kuczyński, T. The theoretical analysis of mass and energy flow through solar collector—Chimney system. *Civ. Environ. Eng. Rep.* **2017**, *24*, 117–131. [CrossRef]
7. Lipnicki, Z.; Gortych, M.; Staszczuk, A.; Kuczyński, T.; Grabas, P. Analytical and Experimental Investigation of the Solar Chimney System. *Energies* **2019**, *12*, 2060. [CrossRef]
8. Schlaich, J. *The Solar Chimney. Electricity from the Sun*; Edition Axel Menges: Stuttgart, Germany, 1995.
9. Mehling, H.; Cobeza, L. *Heat and Cold Storage with PCM*; Springer: Berlin/Heidelberg, Germany, 2008.
10. Lipnicki, Z.; Rubaszewski, A. Współpraca akumulatora ciepła z układem chłodzenia silnika spalinowego. *Arch. Motoryz.* **2000**, *3*, 177–186.
11. Ahmed, O.K.; Algburi, S.; Ali, Z.H.; Ahmed, A.K.; Shubat, H.N. Hybrid solar chimneys: A comprehensive review. *Energy Rep.* **2022**, *8*, 438–460. [CrossRef]
12. Yazdi, M.H.; Solomin, E.; Fudholi, A.; Sopian, K.; Chong, P.L. Numerical analysis of the performance of a hybrid solar chimney system with an integrated external thermal source. *Therm. Sci. Eng. Prog.* **2021**, *26*, 101127. [CrossRef]
13. Behar, O.; Sbarbaro, D.; Morán, L. A Practical Methodology for the Design and Cost Estimation of Solar Tower Power Plants. *Sustainability* **2020**, *12*, 8708. [CrossRef]
14. Albarbar, A.; Arar, A. Performance Assessment and Improvement of Central Receivers Used for Solar Thermal Plants. *Energies* **2019**, *12*, 3079. [CrossRef]
15. Khosravi, A.; Malekan, M.; Pabon, J.J.G.; Zhao, X.; Assad, M.E.H. Design parameter modelling of solar power tower system using adaptive neuro-fuzzy inference system optimized with a combination of genetic algorithm and teaching learning-based optimization algorithm. *J. Clean. Prod.* **2020**, *244*, 118904. [CrossRef]
16. Ahmed, O.K.; Hussein, A.S. New design of solar chimney (case study). *Case Stud. Therm. Eng.* **2018**, *11*, 105–112. [CrossRef]
17. Arzpeyma, M.; Mekhilef, S.; Kazi, S.N.; Horan, B.; Seyedmahmoudian, M.; Akram, N.; Stojcevski, A. Solar chimney power plant and its correlation with ambient wind effect. *J. Therm. Anal. Calorim.* **2019**, *141*, 649–668. [CrossRef]
18. Arzpeyma, M.; Mekhilef, S.; Kazi, S.N.; Horan, B.; Seyedmahmoudian, M.; Akram, N.; Stojcevski, A.; Alnaimat, F.; Mathew, B. Numerical simulation of the effect of chimney configuration on the performance of a solar chimney power plant. *J. Therm. Anal. Calorim.* **2021**, *147*, 2549–2563. [CrossRef]
19. Guo, P.; Li, T.; Xu, B.; Xu, X.; Li, J. Questions and current understanding about solar chimney power plant: A review. *Energy Convers. Manag.* **2018**, *182*, 21–33. [CrossRef]
20. Guo, P.; Wang, Y.; Li, J.; Wang, Y. Thermodynamic analysis of a solar chimney power plant system with soil heat storage. *Appl. Therm. Eng.* **2016**, *100*, 1076–1084. [CrossRef]
21. Habibollahzade, A.; Houshfar, E.; Ashjaee, M.; Ekradi, K. Continuous power generation through a novel solar/geothermal chimney system: Technical/cost analyses and multi-objective particle swarm optimization. *J. Clean. Prod.* **2021**, *283*, 124666. [CrossRef]

22. Tajemnicze Aqda i Nocleg w Świątyni Zoroastrian. Available online: https://kolemsietoczy.pl/tajemnicza-aqda-nocleg-w-swiatyni-zoroastrian/ (accessed on 8 July 2022).
23. Modele Krzepnięcia Materiałów PCM w Różnych Układach Geometrycznych. Available online: https://projekt-energie.eu/pl/platforma-edukacyjna/article-modele-krzepniecia-materialow-pcm-w-roznych-ukladach-geometrycznych.html (accessed on 11 June 2023).
24. RUBITHERM. RT64HC. Available online: https://www.rubitherm.eu/media/products/datasheets/Techdata_-RT64HC_EN_09102020.PDF (accessed on 12 July 2022).
25. Płuciennik-Koropczuk, E.; Myszograj, S.; Mąkowski, M. Reducing CO_2 Emissions from Wastewater Treatment Plants by Utilising Renewable Energy Sources? Case Study. *Energies* **2022**, *15*, 8446. [CrossRef]
26. Myszograj, S.; Bocheński, D.; Mąkowski, M.; Płuciennik-Koropczuk, E. Biogas, Solar and Geothermal Energy—The Way to a Net-Zero Energy Wastewater Treatment Plant—A Case Study. *Energies* **2021**, *14*, 6898. [CrossRef]
27. Kumar, D.; Biswas, N.; Manna, N.K.; Cemal, A. Impact of chimney divergence and sloped absorber on energy efficacy of a solar chimney power plant (SCPP). *Ain Shams Eng. J.* **2024**, *15*, 102390. [CrossRef]
28. Pradhan, S.; Chakraborty, R.; Mandal, D.K.; Barman, A.; Bose, P. Design and performance analysis of solar chimney power plant (SCPP): A review. *Sustain. Energy Technol. Assess.* **2021**, *47*, 101411. [CrossRef]
29. Das, P.; Chandramohan, V.P. A review on solar updraft tower plant technology: Thermodynamic analysis, worldwide status, recent advances, major challenges and opportunities. *Sustain. Energy Technol. Assess.* **2022**, *52*, 102091. [CrossRef]
30. Saleh, M.J.; Atallah, F.S.; Algburi, S.; Ahmed, O.K. Enhancement methods of the performance of a solar chimney power plant: Review. *Results Eng.* **2023**, *19*, 101375. [CrossRef]
31. Taler, J.; Duda, P. *Rozwiązania Prostych i Odwrotnych Zagadnień Przewodzenia Ciepła*; Wydawnictwo Naukowo-Techniczne: Warszawa, Poland, 2003.

Disclaimer/Publisher's Note: The statements, opinions and data contained in all publications are solely those of the individual author(s) and contributor(s) and not of MDPI and/or the editor(s). MDPI and/or the editor(s) disclaim responsibility for any injury to people or property resulting from any ideas, methods, instructions or products referred to in the content.